Zeeman effect of the topological surface states revealed by quantum oscillations up to 91 Tesla

Zuocheng Zhang, Wei Wei, Fangyuan Yang, Zengwei Zhu, Minghua Guo, Yang Feng, Dejing Yu, Mengyu Yao, Neil Harrison, Ross McDonald, Yuanbo Zhang, Dandan Guan, Dong Qian, Jinfeng Jia, and Yayu Wang

Phys. Rev. B **92**, 235402 — Published 1 December 2015

DOI: 10.1103/PhysRevB.92.235402

Zeeman effect of the topological surface states revealed by quantum oscillations up to 91 Tesla

Zuocheng Zhang[1,4*], Wei Wei[2*], Fangyuan Yang[3*], Zengwei Zhu[4], Minghua Guo[1], Yang Feng[1], Dejing Yu[2], Mengyu Yao[2], Neil Harrison[4], Ross McDonald[4], Yuanbo Zhang[3,6], Dandan Guan[2,6], Dong Qian[2,6], Jinfeng Jia[2,6 †], Yayu Wang[1,5†]

[1]*State Key Laboratory of Low Dimensional Quantum Physics, Department of Physics, Tsinghua University, Beijing 100084, China*

[2]*Key Laboratory of Artificial Structures and Quantum Control (Ministry of Education), Department of Physics and Astronomy, Shanghai Jiao Tong University, Shanghai 200240, China*

[3]*State Key Laboratory of Surface Physics and Department of Physics, Fudan University, Shanghai 200433, China*

[4]*National High Magnetic Field Laboratory, Los Alamos National Laboratory, Los Alamos, New Mexico 87545, USA*

[5]*Collaborative Innovation Center of Quantum Matter, Beijing, China*

[6]*Collaborative Innovation Center of Advanced Microstructures, Nanjing University, Nanjing 210093, China*

* *These authors contributed equally to this work.*

† Email: jfjia@sjtu.edu.cn; yayuwang@tsinghua.edu.cn

We report quantum oscillation studies on the $Bi_2Te_{3-x}S_x$ topological insulator single crystals in pulsed magnetic field up to 91 T. For the x = 0.4 sample with the lowest bulk carrier density, the surface and bulk quantum oscillations can be disentangled by combined Shubnikov-de Haas and de Hass-van Alphen oscillations, as well as quantum oscillations in nanometer-thick peeled crystals. At high magnetic field beyond the bulk quantum limit, our results suggest that the zeroth Landau level of topological surface states is shifted due to the Zeeman effect. The *g* factor of the topological surface states is estimated to be between 1.8 and 4.5. These observations shed new light on the quantum transport phenomena of topological insulators in ultrahigh magnetic field.

Three dimensional topological insulators (TIs) have topologically nontrivial bulk band structure and Dirac-like surface states (SSs) protected by the time reversal symmetry (TRS) [1-3]. Breaking the TRS in TI is expected to spawn exotic topological quantum effects and novel spintronic applications. An efficient way to achieve this goal is to create spontaneous ferromagnetic order by means of magnetic doping, which has been demonstrated in the observation of quantum anomalous Hall effect (QAHE) in magnetically doped TI thin films [4-7]. Similarly, we can put the topological SS in close proximity to a ferromagnet [8-10] as proposed for the realization of image magnetic monopoles [11] and inverse spin-galvanic effect [12]. Another powerful TRS-breaking approach is to apply a strong magnetic field perpendicular to the topological SS, which can lead to rich and complex phenomena. On one hand, the orbital motion of Dirac fermions will create discrete Landau levels (LLs) in strong magnetic field. The linear dispersion of the topological SS guarantees that there is a LL pinned at the Dirac point, as demonstrated experimentally [13-17]. This so-called zeroth LL has been actively pursued because it may exhibit remarkable quantum transport phenomena such as the half quantum Hall effect [18-22]. The spin degree of freedom, on the other hand, couples to the magnetic field and gains an extra Zeeman energy. It not only alters the LL distribution, but also opens an energy gap at the Dirac point. Moreover, the quantum Hall ferromagnetism that has been observed in graphene [23,24] and plateau feature in spin magnetization [25] are also expected to occur for the Dirac-like SS in strong magnetic field.

The quantum Hall effect associated with the LL of topological SS has been observed recently in both single crystals [20] and thin films of TI [21]. The existence of the Zeeman effect of the topological SSs, however, is still controversial. Quantum oscillations in strong magnetic field have played an essential role in mapping out the LL spectrum [26-37] and revealing the Zeeman effect of the topological SS [30,33,35,38,39]. Unfortunately, previous reports gave conflicting conclusions regarding the existence of Zeeman effect, and provided dramatically different g factor values for the SS [30,33,35,38,39]. The main complexity comes from the parallel conduction of the bulk states that coexist with or even dominate over the surface transport. Disentangling the surface quantum oscillations from the bulk ones is the prerequisite for revealing the Zeeman effect of topological SS.

In this paper, we study LL quantization in $Bi_2Te_{2.6}S_{0.4}$ TI in pulsed magnetic field up to 91 T. The surface and bulk quantum oscillations can be clearly disentangled by combined Shubnikov-de Haas (SdH) and de Hass-van Alphen (dHvA) oscillations, in conjunction with quantum oscillations in nanometer-thick peeled crystals. At high magnetic field beyond the bulk quantum limit, our results suggest that the zeroth Landau level of topological surface states is shifted due to the Zeeman effect and the *g* factor of the topological surface states is estimated. These observations shed new light on the quantum transport phenomena of TIs and pave the road for the observation of novel quantum effects in ultrahigh magnetic field.

The $Bi_2Te_{3-x}S_x$ single crystals are grown by the self-flux method. Our angle-resolved photoemission spectroscopy (ARPES) experiments were carried out in Advanced Light Source Beamline 4.0.3 with the incident photons of from 70 to 98 eV. All the spectra were taken at 10 K using a Scienta R8000 analyzer. Bulk samples were cleaved at 10 K with a base pressure better than 5×10^{-11} Torr. Magneto transport properties are measured in a perpendicular magnetic field by using standard four-probe ac lock-in method. For the thinnest sample with thickness of 15 nm, the transport measurements are performed in the DC magnet of the National High Magnetic Field Laboratory in Tallahassee with field up to 31 T. The ultrahigh field measurements are performed in the pulsed magnet in Los Alamos. The magnetic susceptibility measurement is taken by using a Seiko piezo-resistive cantilever.

We choose to study sulfur (S) doped Bi_2Te_3 TI single crystals due to their high mobility and tunable Fermi level (E_F) by S content. The insets of Fig. 1a to c display ARPES band maps of three $Bi_2Te_{3-x}S_x$ crystals with x = 1.2, x = 0.7 and 0.4. The Dirac-like topological SSs can be clearly resolved in all three samples. With reducing S content, E_F moves down systematically towards the Dirac point, indicating the reduction of electron-type bulk carriers. In the first two samples, E_F lies within the bulk conduction band but for x = 0.4 sample no bulk band can be detected near E_F. The main panels of Fig. 1a to c display the resistivity (ρ) vs. temperature (T) curves for the three samples. Consistent with the ARPES data, the x = 1.2 and 0.7 samples are metallic over the whole temperature range, and the latter sample has larger resistivity due to reduced bulk carrier density. The x = 0.4 sample, on the other hand, is metallic at high T but shows an upturn for $T < 25$ K.

Figure 2a displays the longitudinal resistivity (ρ_{xx}) and Hall resistivity (ρ_{yx}) of the x = 1.2 sample as a function of perpendicular magnetic field up to 60 T measured at T = 1.5 K. The SdH oscillations can be clearly resolved in both curves. The negative slope of the Hall effect indicates electron-type charge carriers, in agreement with the ARPES measurement that E_F cuts through the conduction band. Fast Fourier transform (FFT) of the ρ_{xx} curves (Fig. 2d) reveals a frequency B_F = 115 T with respect to the inverse magnetic field. The Fermi surface (FS) area A_F can be estimated by the Onsager relation $B_F = \frac{\hbar}{2\pi e}A_F$. Assuming the FS cross section is a simple circle, this FS area corresponds to a Fermi wave vector k_F = 0.059 /Å, which is close to the bulk k_F = (0.050±0.005) /Å revealed by angle resolved photoemission spectroscopy (ARPES) (Fig. 1a). The negative slope of the Hall effect (Fig. 1d) indicates electron-type charge carriers and the carrier density estimated from the low field Hall coefficient is $n = 1.1 \times 10^{19}/cm^3$, which is in broad agreement with the bulk carrier density $7.0 \times 10^{18}/cm^3$ estimated from k_F extracted from quantum oscillations based on an oversimplified spherical FS. Similar SdH oscillations are also observed in the x = 0.7 sample (Fig. 2b), and the frequency is reduced to $B_F = 91$ T (Fig. 2e). Again, the estimated k_F from the FS cross-section is 0.053 /Å, which is consistent with (0.048±0.005) /Å of the bulk conduction band directly measured by ARPES (Fig. 1b).

The x = 0.4 crystal is expected to exhibit distinctively different quantum oscillations patterns because the ARPES measurement show that the E_F lies in the bulk energy gap, thus only the surface states should contribute to the charge transport. Moreover, the ρ vs T curve shows an upturn at low T, again indicating a rather dramatic change of the transport behavior. However, the SdH oscillations shown in Fig. 2c seem to evolve smoothly from that of the previous samples. The slope of the Hall effect becomes larger (Fig. 2c), consistent with a further reduction of nominal carrier density to $3.5 \times 10^{18}/cm^3$. The frequency of the SdH oscillations is merely $B_F = 37$ T (Fig. 2f), indicating a very small FS pocket in the x = 0.4 sample.

It is tempting to ascribe the quantum oscillations in the x = 0.4 sample to the SSs, but temperature dependence of SdH oscillations suggests that they also come from the bulk. Increasing temperature will smear out the Fermi surface and as a result the oscillation amplitude (α) decreases according to the Lifshitz-Kosevich (LK) formula: $\alpha \propto \frac{\chi}{sinh\chi}$, $\chi =$

$\frac{2\pi^2 k_B T}{\hbar\omega_c} = 14.7\frac{m_{cyc}T}{B}$ (Ref. [40]). Here k_B is the Boltzmann constant, $\hbar$ is the Planck constant divided by 2π, $\omega_c = \frac{eB}{m_{cyc}}$ is the cyclotron frequency and m_{cyc} is the cyclotron mass. Therefore, analyzing the temperature decay of the oscillation amplitude allows us to extract the cyclotron mass of the electrons that are responsible for the quantum oscillations. Figure 3a displays the temperature dependence of the SdH oscillations of the x = 0.7 sample, which decreases in amplitude with rising *T*. The solid symbols in Fig. 3b represent the oscillation amplitude at 38.6 T as a function of *T*, which can be fitted very well by using the LK formula (red solid line). The extracted $m_{cyc} = 0.19\, m_0$, m_0 is the free electron mass, agrees very well with previous studies on the bulk of TIs [41,42]. Figure 3c displays the temperature evolution of the oscillation amplitude of the x = 0.4 sample, which is very similar to that of the x = 0.7 sample. The LK formula fit of the amplitude decay of a particular oscillation also generates a $m_{cyc} = 0.19\, m_0$, which is identical to that of the x = 0.7 sample (Fig. 3d).

The $B_F = 37$ T SdH oscillations in the x = 0.4 crystal also originate from the bulk states, which can be confirmed by dHvA oscillations measured by torque magnetometer. Because of the limited magnetic moment contribution of SSs, only bulk quantum oscillations can be detected by the magnetometer in pulsed magnet. Fig. 4a shows the field dependence of the torque measured on the x = 0.7 sample, which exhibits clear oscillations at high field. Fig. 4a inset shows the negative derivative of the torque data (blue), which matches very well with the resistivity curve (black). For the x = 0.4 sample, Fig. 4b shows that dHvA oscillations can be detected in magnetic field up to around 37 T. The derivative of the torque data (blue) also matches the resistivity curve. However, with further increase of magnetic field the torque signal shows a steep increase with no sign of oscillation or saturation up to 60 T. This indicates that a magnetic field near $B_F = 37$ T is sufficient to squeeze all the bulk electrons to the lowest LL, and there is no more bulk quantum oscillations at higher magnetic field. Our experiments clearly demonstrate that even ARPES detects no bulk FS at E_F of the x = 0.4 sample, the bulk states can still make significant contributions to transport. The most likely explanation for the discrepancy between ARPES and transport measurements is the band bending effect at the sample surface [41]. Therefore, the ARPES and transport results thus provide complementary information regarding the electronic structure of the TI. The

exposure to atmosphere when performing *ex situ* transport measurements could also be responsible for such inconsistency.

For magnetic field beyond the bulk quantum limit, the quantum oscillations should originate solely from the SSs. This provides a good opportunity for us to probe the LL spectrum of the SSs, but a significantly larger magnetic field is needed. To fulfill this task, we carried out transport measurements in pulsed magnetic field up to 91 T. The magnetoresistance (MR) and Hall effect are shown in Fig. 5a and 5b. Another peak and valley in MR are observed for $\mu_0 H$ > 35 T, and at the same time the Hall resistance keeps increasing up to 91 T. The estimated Hall angle θ by $tan\theta = \frac{R_{yx}}{R_{xx}}$ is around 87 degrees in the ultrahigh magnetic field. Given the condition of observing SdH oscillations ($B\mu_b >> 1$), the bulk mobility μ_b is around 1500 cm^2/Vs since bulk oscillations start around 7 T. The magnetoconductance (MC) and Hall conductance can be calculated from ρ_{xx} and ρ_{yx} by using the tensor relation $\sigma_{xx} = \frac{\rho_{xx}}{\rho_{xx}^2+\rho_{yx}^2}, \sigma_{xy} = \frac{\rho_{yx}}{\rho_{xx}^2+\rho_{yx}^2}$. The magnetic field dependence of σ_{xx} and σ_{xy} at 4.3 K are shown in Fig. 5c. At high magnetic field, σ_{xx} drops by two orders of magnitude from its zero field value, suggesting the suppression of bulk conduction. Beyond the bulk quantum limit, σ_{xy} develops a plateau above 78 T, at which a minimum is observed in σ_{xx}.

Another way to directly probe the surface quantum oscillations is to reduce the sample thickness to enhance the surface to bulk ratio so that the SSs dominate the transport process. To achieve this goal, we mechanically peel the x = 0.4 crystal down to 15 nm. As shown in Fig. 6a, with decreasing thickness, the resistance value increases systematically due to the reduced bulk contribution. In contrast with the low field parabolic MR shown in Fig. 5a, the MR of the 15 nm thick sample shown in Fig. 6b displays a sharp positive cusp at low magnetic field, which is the weak antilocalization behavior characteristic of the topological SSs due to the non-trivial Berry phase [43-46]. At high magnetic field MR starts to oscillate at around 20 T and thus the estimated mobility μ_s of SSs is around 500 cm^2/Vs, which is lower than the bulk 1500 cm^2/Vs mobility. As shown in Fig. 6c, the frequency estimated by the slope of the linear fit to the LL index is around 157 T and the intercept of the linear fit is -

0.49, confirming the non-trivial Berry phase. More importantly, the extracted k_F value from the 157 T oscillation frequency is 0.069 /Å, which matches perfectly with the k_F of SS revealed by the ARPES data shown in Fig. 1c inset. This is strong evidence that the high frequency quantum oscillations originate from the topological SSs.

The disentanglement of bulk and surface quantum oscillations, as well as the reliable assignment of the surface LL index at strong magnetic field, allows us to address the Zeeman effect of the topological SSs. The presence of Zeeman energy adds a massive term in the Landau quantization, as a result the LL energy can be expressed as [30,35]:

$$E_N(B) = \pm\sqrt{2N\hbar v_F^2 eB + \left(\frac{g_s\mu_B|B|}{2}\right)^2} \text{ with } N = \pm1, \pm2\cdots \quad (1).$$

Here v_F is the Fermi velocity, g_s is the g-factor of the SSs, μ_B is the Bohr magneton, and $\pm$ denotes the hole- and electron-like Dirac fermions. For the zeroth LL with $N = 0$, its energy is shifted to $E_N(B) = \frac{g_s\mu_B|B|}{2}$. Up to date, Zeeman shift of the zeroth LL and the g-factor of the surface Dirac fermions are still controversial. The reported g-factor value varies widely from 2 (Ref. [35]) to 76 (Ref. [38]).

The main source of discrepancy regarding the Zeeman shift originates from the assignment of the LL occupancy. Our surface quantum oscillation measurements up to 91 T enable a more reliable determination of the shift of the zeroth LL. Because the SS k_F extracted from quantum oscillations and ARPES measurement is around k_F = 0.069/Å, the surface carrier density equals $\frac{k_F^2}{4\pi} = 3.74 \times 10^{12}/cm^2$ if we assume a simple circular FS for one spin-polarized Dirac cone. On the other hand, at 78 T each spin-polarized LL of the SS can accommodate $\frac{B}{h/e} = 1.87 \times 10^{12}/cm^2$ carriers, thus two surface LLs are fully occupied at 78 T. A more straightforward way to estimate the LL filling factor is the quantum oscillations in the 15 nm thick sample reveals a 157 T frequency for the topological SSs, hence two LLs will be fully occupied at 78 T. In the MC measured up to 91 T, we observe a MC minimum at around 78 T, which is perfectly consistent with the occupancy of two integer LLs. As schematically shown in Fig. 7b, the integer LL filling indicates that the center of the zeroth LL is no longer pinned at the Dirac point, but is shifted upwards by the Zeeman effect.

The Zeeman shift of zeroth LL in nonmagnetic TI has not been observed before due to the inadequate magnetic field that has been applied [20,35]. Our work in ultrahigh magnetic field provides the first experimental evidence for the Zeeman shift of the zeroth LL.

Next we give an estimate of the g factor of the topological SS. In our experiment, two integer LLs are exactly occupied at 78 T. This implies that the Zeeman energy $\frac{g_s\mu_B|B|}{2}$ at 78 T should be larger than half of the LL broadening (Fig. 5b), because otherwise only a fraction of the zeroth LL is occupied. This observation gives the lower limit for the g-factor. On the other hand, the surface quantum oscillation patterns up to 31 T (Fig. 3a) are not affected by the Zeeman effect and still has an intercept close to half-integer. This sets the upper limit for the g-factor because it indicates the Zeeman energy at 30 T is much smaller than the half of LL broadening.

The energy scale of Dingle temperature k_BT_D reflects the LL broadening [40], which can be estimated by performing Dingle analysis. The magnetic field dependence of oscillation amplitude can be expressed as $A_s \propto \frac{\chi_s}{sinh\chi_s} e^{\frac{-\chi_s T_D}{T}}$, $\chi_s = \frac{2\pi^2 k_B T}{\hbar\omega_s} = 14.7\frac{m_D T}{B}$ (Ref. [40]). Here A_s is the oscillation amplitude of the topological SSs, T_D is the Dingle temperature, $\omega_s = \frac{eB}{m_D}$ is the cyclotron frequency, $m_D = \frac{E_F}{v_F^2}$ is the cyclotron mass (extracted from the ARPES measurement), k_B is the Boltzmann constant, $\hbar$ is the Planck constant divided by 2π. Fig. 7a displays three discreet points of $\ln(A_sBsinh(14.7m_DT/B))$ with respect to inverse magnetic field. The slope of the linear fit (red curve in Fig. 7a) directly generates the Dingle temperature T_D, which is 92 K for this x = 0.4 sample. From the above analysis, the estimated g-factor of the topological SS is larger than 1.8 and smaller than 4.5, which is similar to the reported value in graphene [23,47]. Such a small g factor suggests that the Zeeman effect of topological SS is unimportant to the quantum transport behavior unless in an ultrahigh magnetic field. This also explains why previous STM experiments at 11 T cannot resolve the Zeeman shift (Ref. [13,14]).

In summary, transport measurements up to 91 T as well as the striking contrast between torque and transport measurements allow us to disentangle the quantum oscillations from the

coexisting bulk and surface states in $Bi_2Te_{2.6}S_{0.4}$. The LL occupancy analysis in the extreme quantum limit suggests Zeeman shift of the zeroth LL of the SS and the *g* factor is estimated to be between 1.8 and 4.5. Its small value indicates that the Zeeman effect is insignificant in most experiments on TI, but becomes relevant in ultrahigh magnetic field. These results pave the way for the realization of novel phenomenon such as the quantum Hall ferromagnetism in which Zeeman effect of the zeroth LL plays an essential role [23,24].

Acknowledgements

This work is supported by NSFC and MOST of China (grant number 2015CB921000, 2013CB921900). The Advanced Light Source is supported by the Director, Office of Science, Office of Basic Energy Sciences, of the US Department of Energy under Contract No. DE-AC02-05CH11231. D.Q. acknowledges additional supports from the Top-notch Young Talents Program. The high field measurements were supported by the University of California UCOP grant 'Quantum Phenomena in Topological Insulators' and the US Department of Energy BES grant 'Science of 100 tesla'.

Figure Captions:

Fig. 1. a-c, The ARPES band maps and temperature dependence of resistivity curves for the x = 0.4 (a), 0.7 (b) and 1.2 (c) single crystals.

Fig. 2. a-c, The SdH oscillations for the x = 0.4 (a), 0.7 (b) and 1.2 (c) samples. d-f, Fast Fourier transform for the SdH oscillations in the x = 0.4 (d), 0.7 (e) and 1.2 (f) samples.

Fig. 3. a,c, Temperature dependence of ρ_{xx} for the x = 0.7 (a) and x = 0.4 (c) samples. Each curve is offset by 0.8 mΩ cm in (a) and (c) for clarity. b,d. The absolute SdH oscillation amplitude as a function of T for the x = 0.7 (b) and x = 0.4 (d) samples.

Fig. 4. Magnetic field dependence of torque measurements for the x = 0.7 (a) and 0.4 (b) samples. The inset shows that the negative derivative of torque signal perfectly matches with the resistivity curves.

Fig. 5. Magnetoresistance (a) and Hall effect (b) of the x = 0.4 sample measured in the 91 T pulsed magnet field. c, The magnetoconductance and Hall conductance up to 91 T converted from the data shown in (a) and (b).

Fig. 6. a, Thickness dependence of resistance for the 15 nm, 33 nm and 75 nm thick x = 0.4 peeled crystals. b, Magnetoresistance in the 15 nm thick sample. c, The Landau fan diagram generates a 157 T oscillation frequency and a -0.49 intercept.

Fig. 7. a, The Dingle analysis of the SdH oscillations in the 15 nm thick sample. b, The schematic LL occupancy without and with the Zeeman shift of the zeroth LL of the topological surface states.

References:

[1] X.-L. Qi and S.-C. Zhang, Phys. Today **63**, 33-38 (2010).

[2] M. Z. Hasan and C. L. Kane, Rev. Mod. Phys. **82**, 3045-3067 (2010).

[3] J. E. Moore, Nature **464**, 194-198 (2010).

[4] C.-Z. Chang, J. Zhang, X. Feng, J. Shen, Z. Zhang, M. Guo, K. Li, Y. Ou, P. Wei, L.-L. Wang, Z.-Q. Ji, Y. Feng, S. Ji, X. Chen, J. Jia, X. Dai, Z. Fang, S.-C. Zhang, K. He, Y. Wang, L. Lu, X.-C. Ma, and Q.-K. Xue, Science **340**, 167-170 (2013).

[5] J. G. Checkelsky, R. Yoshimi, A. Tsukazaki, K. S. Takahashi, Y. Kozuka, J. Falson, M. Kawasaki, and Y. Tokura, Nat. Phys. **10**, 731-736 (2014).

[6] X. Kou, S.-T. Guo, Y. Fan, L. Pan, M. Lang, Y. Jiang, Q. Shao, T. Nie, K. Murata, J. Tang, Y. Wang, L. He, T.-K. Lee, W.-L. Lee, and K. L. Wang, Phys. Rev. Lett. **113**, 137201 (2014).

[7] C.-Z. Chang, W. Zhao, D. Y. Kim, H. Zhang, B. A. Assaf, D. Heiman, S.-C. Zhang, C. Liu, M. H. W. Chan, and J. S. Moodera, Nat. Mater. **14**, 473-477 (2015).

[8] M. Lang, M. Montazeri, M. C. Onbasli, X. Kou, Y. Fan, P. Upadhyaya, K. Yao, F. Liu, Y. Jiang, W. Jiang, K. L. Wong, G. Yu, J. Tang, T. Nie, L. He, R. N. Schwartz, Y. Wang, C. A. Ross, and K. L. Wang, Nano Lett. **14**, 3459-3465 (2014).

[9] Q. I. Yang, M. Dolev, L. Zhang, J. Zhao, A. D. Fried, E. Schemm, M. Liu, A. Palevski, A. F. Marshall, S. H. Risbud, and A. Kapitulnik, Phys. Rev. B **88**, 081407 (2013).

[10] P. Wei, F. Katmis, B. A. Assaf, H. Steinberg, P. Jarillo-Herrero, D. Heiman, and J. S. Moodera, Phys. Rev. Lett. **110**, 186807 (2013).

[11] X.-L. Qi, R. Li, J. Zang, and S.-C. Zhang, Science **323**, 1184-1187 (2009).

[12] I. Garate and M. Franz, Phys. Rev. Lett. **104**, 146802 (2010).

[13] P. Cheng, C. Song, T. Zhang, Y. Zhang, Y. Wang, J. F. Jia, J. Wang, Y. Wang, B. F. Zhu, X. Chen, X. C. Ma,

K. He, L. L. Wang, X. Dai, Z. Fang, X. Xie, X. L. Qi, C. X. Liu, S. C. Zhang, and Q. K. Xue, Phys. Rev. Lett. **105**, 076801 (2010).

[14] T. Hanaguri, K. Igarashi, M. Kawamura, H. Takagi, and T. Sasagawa, Phys. Rev. B **82**, 081305 (2010).

[15] Y. Jiang, Y. Wang, M. Chen, Z. Li, C. Song, K. He, L. Wang, X. Chen, X. Ma, and Q.-K. Xue, Phys. Rev. Lett. **108**, 016401 (2012).

[16] Y. Okada, W. Zhou, C. Dhital, D. Walkup, Y. Ran, Z. Wang, S. Wilson, and V. Madhavan, Phys. Rev. Lett. **109**, 166407 (2012).

[17] R. Yoshimi, A. Tsukazaki, K. Kikutake, J. G. Checkelsky, K. S. Takahashi, M. Kawasaki, and Y. Tokura, Nat. Mater. **13**, 253-257 (2014).

[18] X. L. Qi, T. L. Hughes, and S. C. Zhang, Phys. Rev. B **78**, 195424 (2008).

[19] C. Brüne, C. X. Liu, E. G. Novik, E. M. Hankiewicz, H. Buhmann, Y. L. Chen, X. L. Qi, Z. X. Shen, S. C. Zhang, and L. W. Molenkamp, Phys. Rev. Lett. **106**, 126803 (2011).

[20] Y. Xu, I. Miotkowski, C. Liu, J. Tian, H. Nam, N. Alidoust, J. Hu, C.-K. Shih, M. Z. Hasan, and Y. P. Chen, Nat. Phys. **10**, 956-963 (2014).

[21] R. Yoshimi, A. Tsukazaki, Y. Kozuka, J. Falson, K. S. Takahashi, J. G. Checkelsky, N. Nagaosa, M. Kawasaki, and Y. Tokura, Nat. Commun. **6**, 6627 (2015).

[22] C. Brüne, C. Thienel, M. Stuiber, J. Böttcher, H. Buhmann, E. G. Novik, C.-X. Liu, E. M. Hankiewicz, and L. W. Molenkamp, Phys. Rev. X **4**, 041045 (2014).

[23] A. F. Young, C. R. Dean, L. Wang, H. Ren, P. Cadden-Zimansky, K. Watanabe, T. Taniguchi, J. Hone, K. L. Shepard, and P. Kim, Nat. Phys. **8**, 550-556 (2012).

[24] K. Lee, B. Fallahazad, J. Xue, D. C. Dillen, K. Kim, T. Taniguchi, K. Watanabe, and E. Tutuc, Science **345**, 58-61 (2014).

[25] M. M. Vazifeh and M. Franz, Phys. Rev. B **86**, 045451 (2012).

[26] A. A. Taskin and Y. Ando, Phys. Rev. B **80** (2009).

[27] J. G. Checkelsky, Y. S. Hor, M. H. Liu, D. X. Qu, R. J. Cava, and N. P. Ong, Phys. Rev. Lett. **103**, 246601 (2009).

[28] Z. Ren, A. A. Taskin, S. Sasaki, K. Segawa, and Y. Ando, Phys. Rev. B **82**, 241306 (2010).

[29] D. X. Qu, Y. S. Hor, J. Xiong, R. J. Cava, and N. P. Ong, Science **329**, 821-824 (2010).

[30] J. G. Analytis, R. D. McDonald, S. C. Riggs, J. H. Chu, G. S. Boebinger, and I. R. Fisher, Nat. Phys. **6**, 960-964 (2010).

[31] A. A. Taskin, K. Segawa, and Y. Ando, Phys. Rev. B **82** (2010).

[32] Z. Ren, A. A. Taskin, S. Sasaki, K. Segawa, and Y. Ando, Phys. Rev. B **84** (2011).

[33] A. A. Taskin, Z. Ren, S. Sasaki, K. Segawa, and Y. Ando, Phys. Rev. Lett. **107**, 016801 (2011).

[34] B. Sacépé, J. B. Oostinga, J. Li, A. Ubaldini, N. J. G. Couto, E. Giannini, and A. F. Morpurgo, Nat. Commun. **2**, 575 (2011).

[35] J. Xiong, Y. Luo, Y. Khoo, S. Jia, R. J. Cava, and N. P. Ong, Phys. Rev. B **86**, 045314 (2012).

[36] J. Xiong, Y. Khoo, S. Jia, R. J. Cava, and N. P. Ong, Phys. Rev. B **88**, 035128 (2013).

[37] Y. Ando, J. Phys. Soc. Jpn. **82**, 102001 (2013).

[38] A. A. Taskin and Y. Ando, Phys. Rev. B **84**, 035301 (2011).

[39] A. R. Wright and R. H. McKenzie, Phys. Rev. B **87**, 085411 (2013).

[40] D. Shoenberg, *Magnetic Oscillations in Metals* (Cambridge University Press, Cambridge, 1984).

[41] J. G. Analytis, J.-H. Chu, Y. Chen, F. Corredor, R. D. McDonald, Z. X. Shen, and I. R. Fisher, Phys. Rev. B **81**, 205407 (2010).

[42] H. Cao, J. Tian, I. Miotkowski, T. Shen, J. Hu, S. Qiao, and Y. P. Chen, Phys. Rev. Lett. **108**, 216803 (2012).

[43] J. Chen, H. J. Qin, F. Yang, J. Liu, T. Guan, F. M. Qu, G. H. Zhang, J. R. Shi, X. C. Xie, C. L. Yang, K. H. Wu, Y. Q. Li, and L. Lu, Phys. Rev. Lett. **105**, 176602 (2010).

[44] M. Liu, C. Chang, Z. C. Zhang, Y. Zhang, W. Ruan, K. He, L. L. Wang, X. Chen, J. F. Jia, S. C. Zhang, Q. K. Xue, X. C. Ma, and Y. Y. Wang, Phys. Rev. B **83**, 165440 (2011).

[45] H.-Z. Lu, J. Shi, and S.-Q. Shen, Phys. Rev. Lett. **107**, 076801 (2011).

[46] Y. S. Kim, M. Brahlek, N. Bansal, E. Edrey, G. A. Kapilevich, K. Iida, M. Tanimura, Y. Horibe, S.-W. Cheong, and S. Oh, Phys. Rev. B **84**, 073109 (2011).

[47] Y. Zhang, Z. Jiang, J. P. Small, M. S. Purewal, Y. W. Tan, M. Fazlollahi, J. D. Chudow, J. A. Jaszczak, H. L. Stormer, and P. Kim, Phys. Rev. Lett. **96**, 136806 (2006).

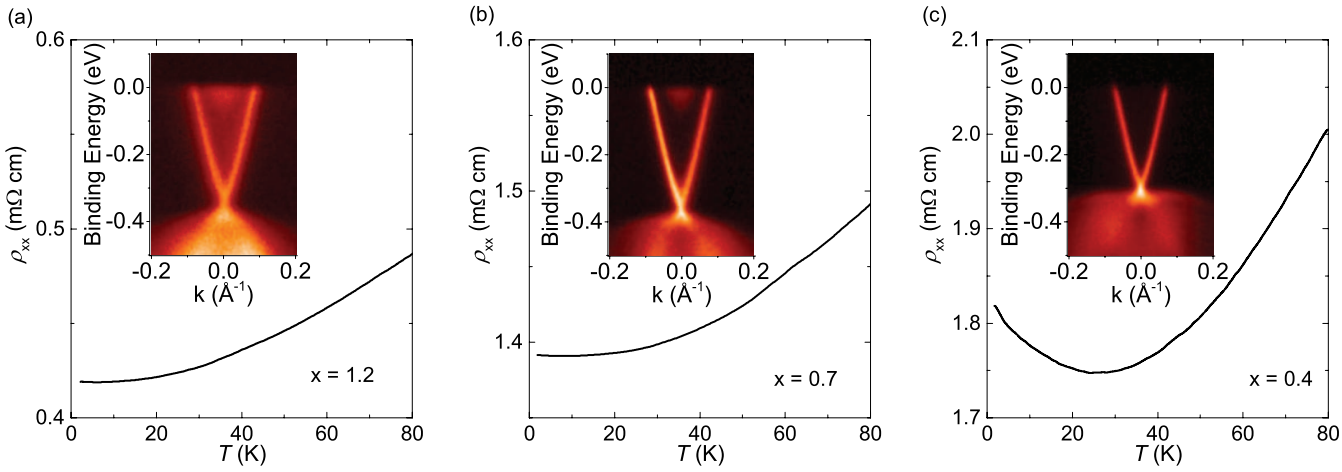

Figure 1 LE15449 06NOV15

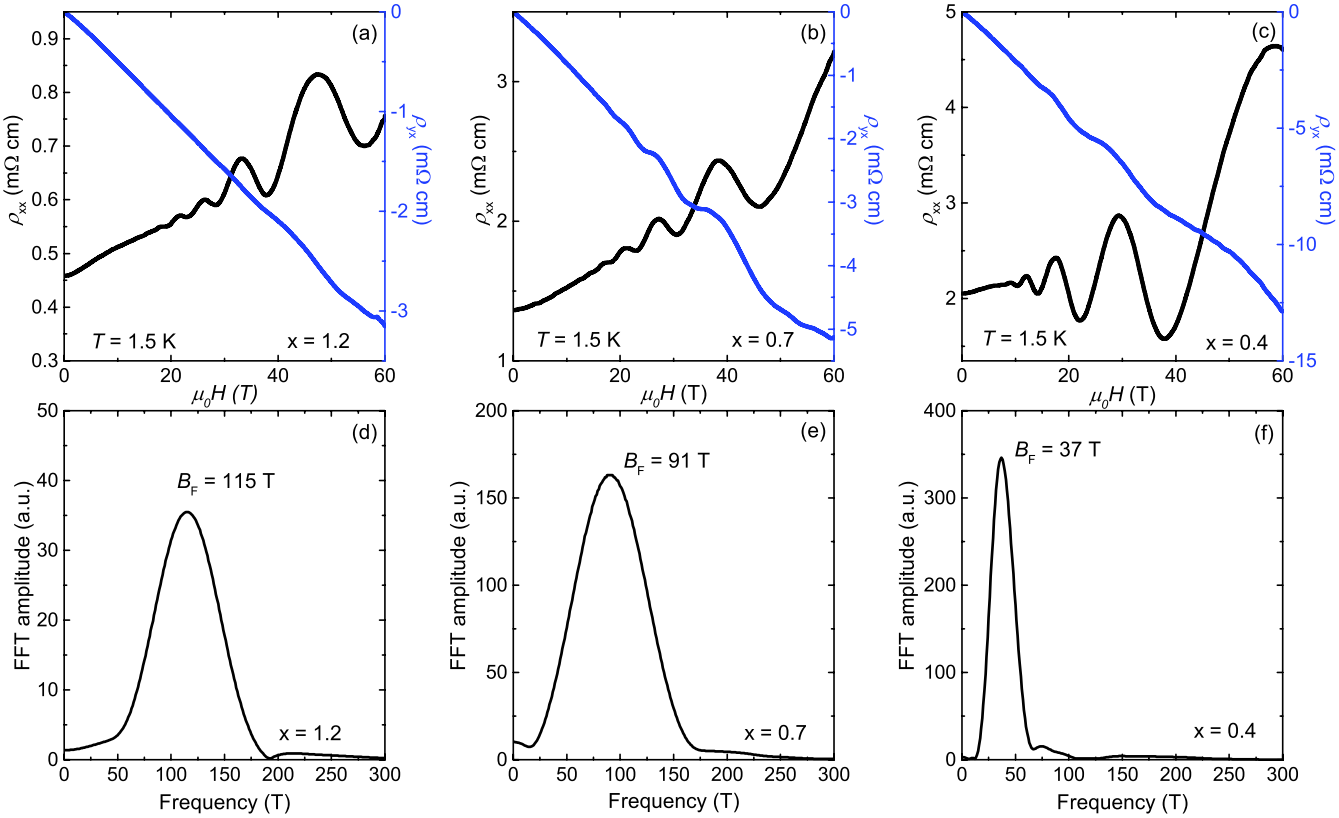

Figure 2 LE15449 06NOV15

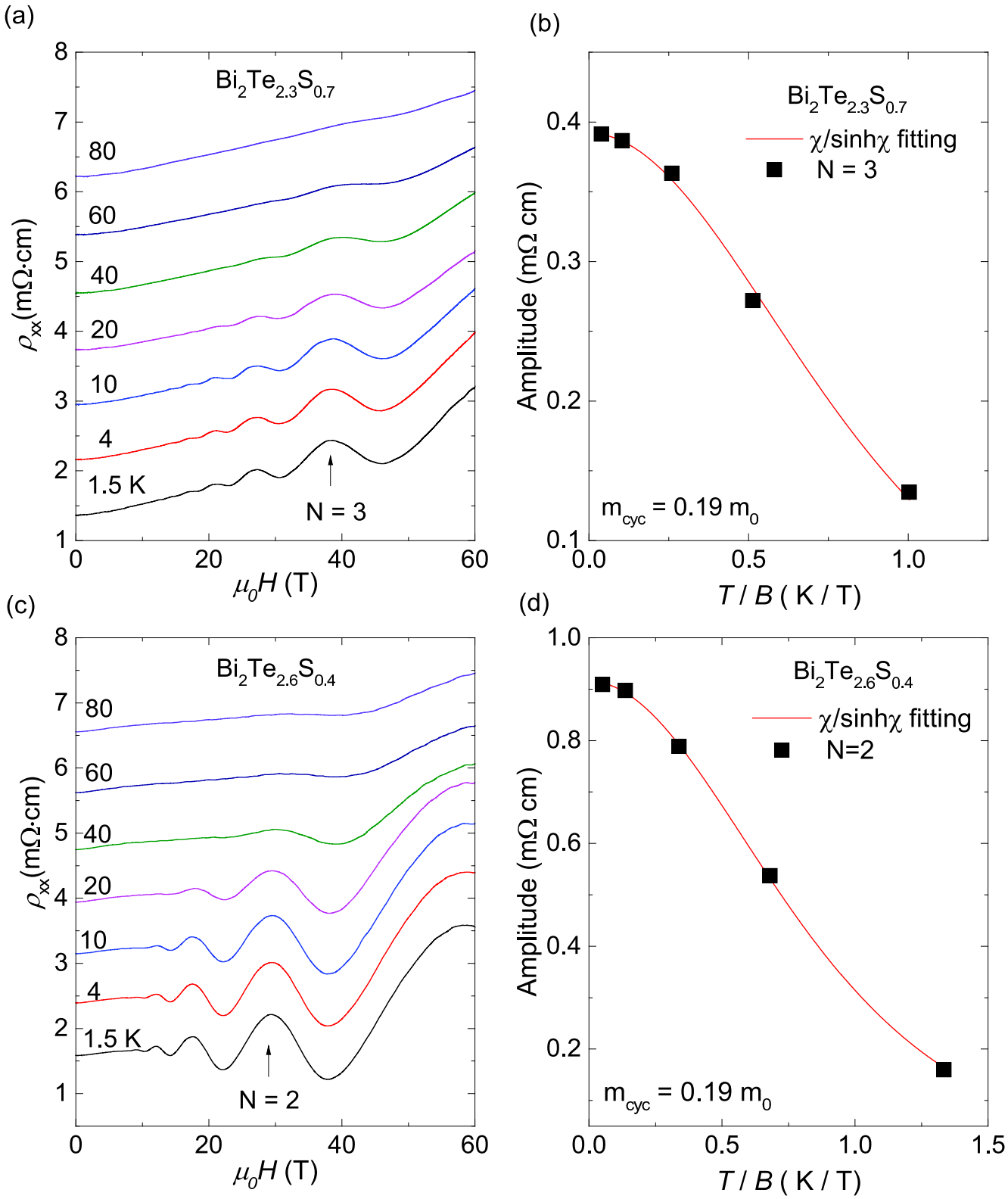

Figure 3 LE15449 06NOV15

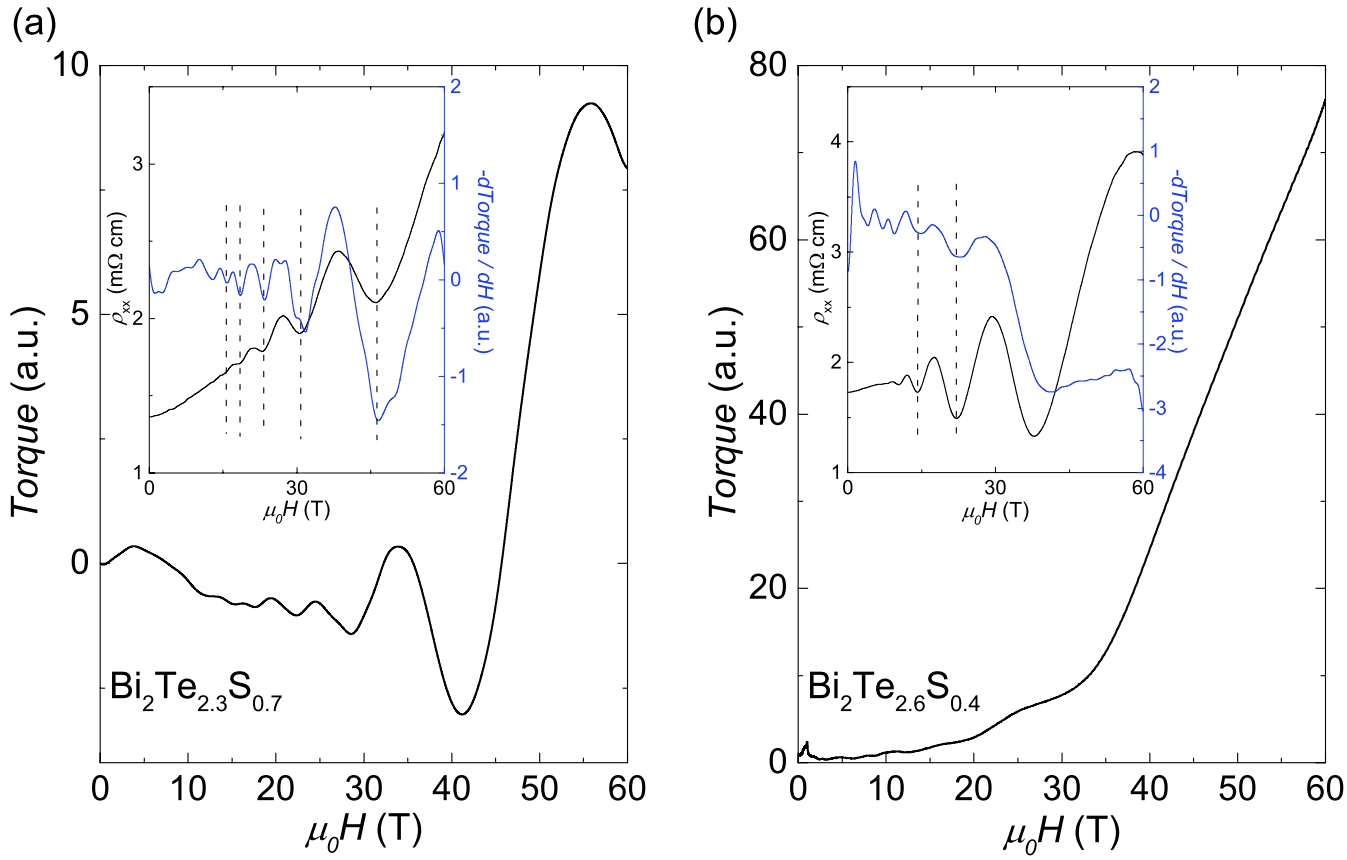

Figure 4 LE15449 06NOV15

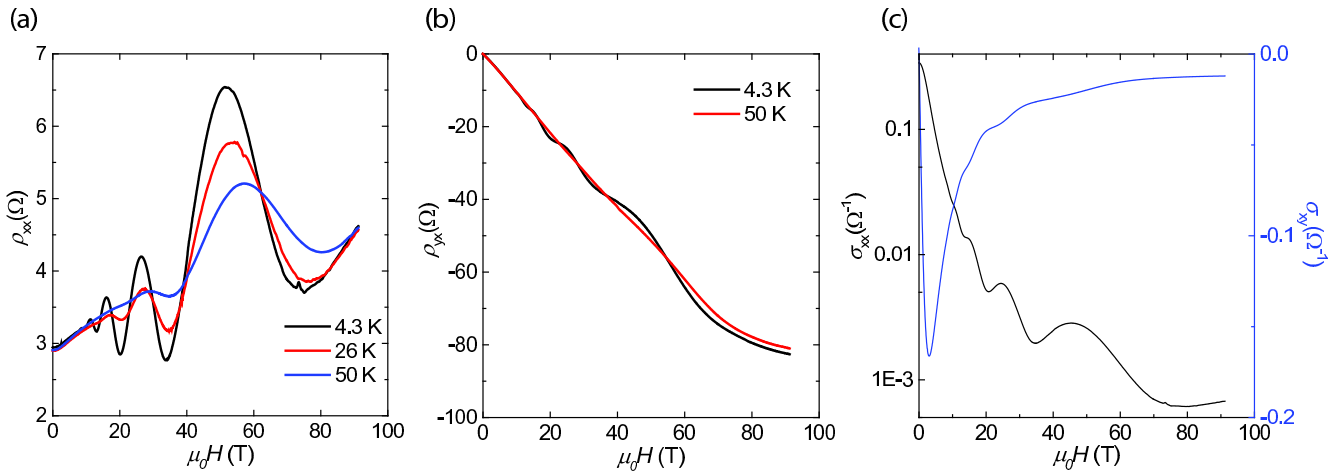

Figure 5 LE15449 06NOV15

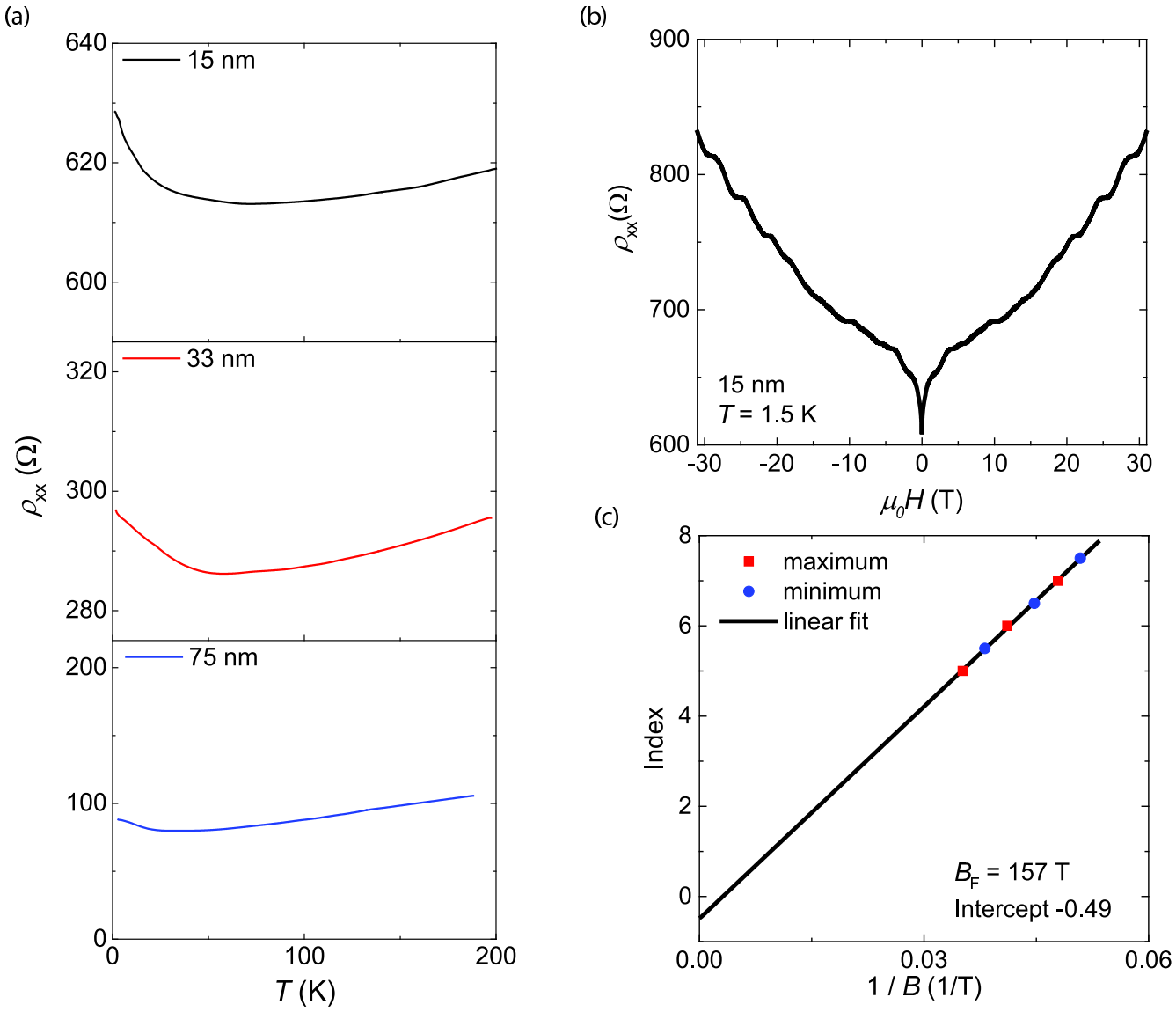

Figure 6 LE15449 06NOV15

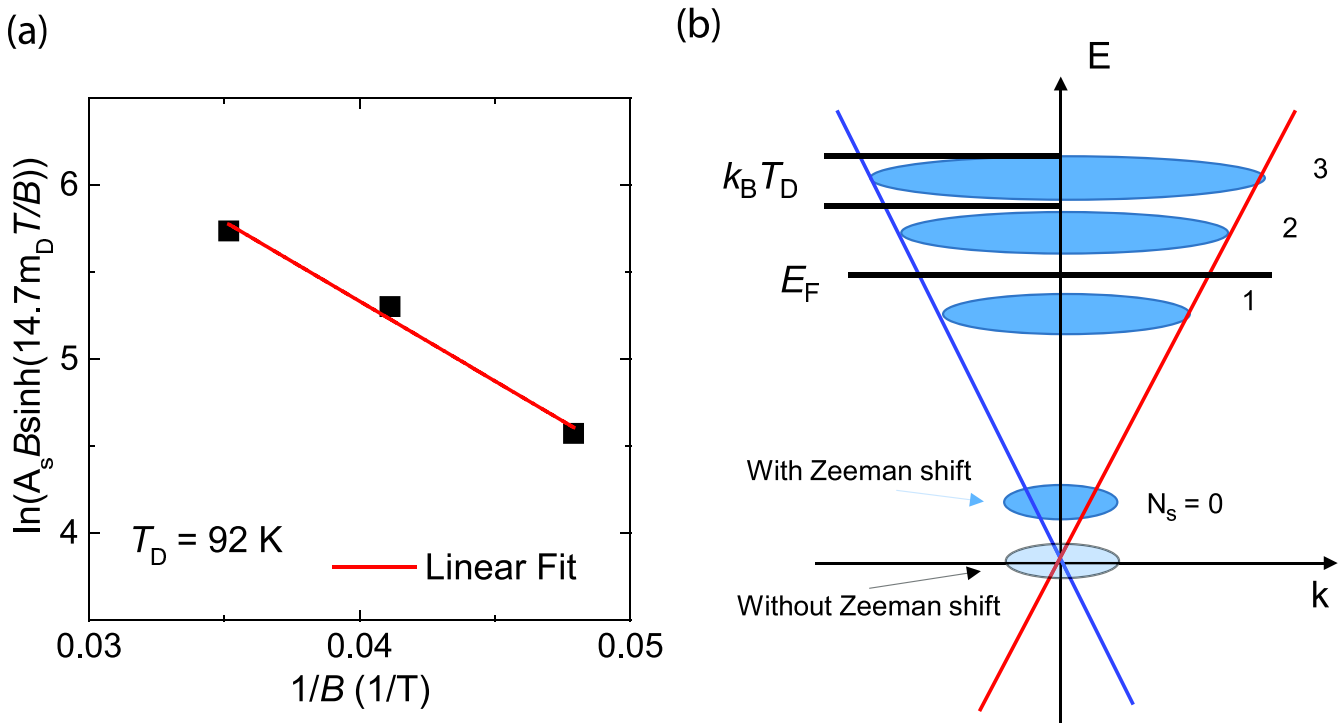

Figure 7 LE15449 06NOV15